

Structural and optical properties of Mn₂O₃ nanoparticles & its gas sensing applications

Shiva Sharma^{1*}, Pratima Chauhan¹, Shahid Husain²

¹Department of Physics, University of Allahabad, Allahabad, 211002, India

²Department of Physics, Aligarh Muslim University, Aligarh, 202002, India

*Corresponding author, E-mail: shivasharmaau@gmail.com, mangu167@gmail.com; Tel: (0532) 2460993

Received: 31 March 2016, Revised: 03 August 2016 and Accepted: 03 September 2016

DOI: 10.5185/amp.2016/220

www.vbripress.com/amp

Abstract

Mn₂O₃ nanoparticles have been synthesized using chemical co-precipitation method. The as synthesized nanoparticles were characterized by X-ray diffractometer (XRD), UV-Visible spectrophotometer (UV-Vis) and Fourier Transform Infra-Red (FTIR) spectrophotometer method. The results indicate that synthesized Mn₂O₃ nanoparticles possessed crystallites having sizes 12.56 nm and 11.90 nm with cubic and orthorhombic structures respectively. The two samples are named as M1 and M2. The gas response of both the samples was investigated for different concentrations of NH₃ gas at room temperature. Sample M2 based thick film sensor showed enhanced sensing performance in comparison to sample M1. This is attributed to smaller crystallite size of sample M2. The sample M2 based sensor showed the response of 67.1% with the response and recovery times 65 and 71 sec respectively. The fabricated nanoparticles show promising use as room temperature NH₃ sensors. Copyright © 2016 VBRI Press.

Keywords: Mn₂O₃, thick films, nanoparticles, NH₃ sensor, polyvinyl pyrrolidone.

Introduction

Urbanization and industrial growth have resulted in severe health issues for the living beings because of increased pollution. Hence, there is an urgent need for developing devices which can monitor pollution level and hence raise an alarm for the immediate control before actual damage is done to the mankind in the surrounding region. In recent decades, many scientists and researchers have focused their attention on developing such devices to detect the presence of unwanted entities in the environment by using nanotechnology. Nanoscale materials provide numerous advantages over bulk in respect of high surface to volume ratio and hence suggest their applications in wide areas such as catalysis, optics, electronics, varistors, detectors and ceramics etc. [1-3]. Semiconductor oxide based sensors is a thrust area of research offering several advantages in comparison to other sensors in respect of their low cost, compact size, fast response and recovery times, good stability and affordability [4-6]. A lot of work has been reported on sensing devices based on TiO₂, WO₃ and Fe₂O₃ [7-9].

Several methods have been utilized for fabricating nanomaterial such as hydrothermal, co-precipitation, pulsed laser ablation, electrochemical, sol-gel [10-14] etc. Among them, chemical co-precipitation method

is the simplest and economical. This method provides good control of both composition and particle size.

During synthesis process, use of surfactant plays a key role in controlling particle size, stabilizing the particles and in preventing them from agglomeration.

A range of gases such as LPG, ammonia (NH₃), carbon monoxide (CO), hydrogen sulfide (H₂S), Organic vapors etc. shows a direct impact on human beings due to their toxicity, occurrence, and persistence in the environment [15-19]. Among the above gases, detection of NH₃, a colorless, poisonous gas with reducing behavior, is most important. There are several sources of ammonia in air such as decomposition process of manure, chemical industry for fertilizers productions, refrigeration systems etc. Its leakage at high concentration can be very dangerous for the environment as well as for living beings. Several researchers have synthesized semiconductor metal oxides and composites like PdS/TiO, ZnO, Co₃O₄/SnO₂ etc. and explored them NH₃ gas sensing [20-22]. However, the sensitivity with good response at lower temperature remains the main challenge for these materials. Hence there is a persistent need for an NH₃ sensor with improved response and recovery time at optimum working temperature. Another important challenge is repeatability. The gas sensing properties of a sensor are based on the change in the electrical resistivity of

a semiconducting metal oxide on interaction with the gas. This change occurs due to the interaction between examined gas molecules and the surface atoms of the sensor materials [23-24].

In recent years, manganese oxides have received great attention and demonstrated to be a good material for use in electrochemical sensors. Manganese oxides exhibit different structures and phases having different oxidation states (+2, +3, +4) like MnO, MnO₂, Mn₂O₃, Mn₃O₄, and Mn₅O₈ which help in showing good gas sensing properties. Such materials possess specific magnetic, structural and transport properties [25-26]. These materials have variable conductivity range from $10^{-6} \Omega^{-1} \text{cm}^{-1}$ to $10^3 \Omega^{-1} \text{cm}^{-1}$ [27]. Such properties are of considerable interest from the experimental point of view. Experimentally it has been reported that MnO nanoclusters show ferromagnetic character while antiferromagnetic nature is possessed by bulk MnO [28]. The above-defined properties can also be modified by controlling the particle size and synthesis methods [29]. Despite the above-defined properties, Manganese oxide with different oxidation states shows their promising response towards several toxic gases and pollutant impurities. Many researchers synthesized manganese oxide materials and analyzed them for gas sensing applications [30-31].

In this paper, we are reporting the synthesis and characterization of Manganese oxide nanoparticles for use in NH₃ gas sensing. The structural and optical properties of these were analyzed by X-ray diffraction and UV-Visible spectroscopy, Fourier Transform Infra-red spectroscopy respectively. The NH₃ sensing characteristics of both sensors M1 and M2 were analyzed as a function of the NH₃ concentration at room temperature. To the best of our knowledge, this is the first report to the use of Mn₂O₃ for sensing NH₃ gas at room temperature.

Experimental

Materials

Manganous acetate [(CH₃COO)₂Mn.4H₂O], Sodium hydroxide pellets (NaOH), Hydrochloric acid (HCl), Poly-Vinyl Pyrrolidone (PVP) used for the synthesis of Mn₂O₃ nanoparticles were purchased from Rankem chemical co. with 99.00% purity.

Synthesis of Nanoparticles

Chemical co-precipitation process was used to prepare Mn₂O₃ nanoparticles. A mixture of 0.1M sodium hydroxide (NaOH) with 1.5 wt % Polyvinyl pyrrolidone (PVP) was prepared in 50 ml distilled water with continuous stirring. A 0.1M solution of manganous acetate prepared in distilled water was added to the above solution with continuous stirring until the color of solution was changed from bright yellow color to dark brown color and left in static age for 24 hours. The settled precipitate was filtered

and dried at room temperature. The final product was named as sample M1 after calcination at 550°C.

In second step, a solution of 0.1M manganous acetate was prepared in 100 ml distilled water and a prepared mixture of 1.5 % wt PVP and 50 ml hydrochloric acid was added to it with continuous stirring and heated at 80 °C until the color of solution was changed from bright yellow color to dark brown color and product was left for 24 hours in static age. In this case, hydrochloric acid was used as a reducing agent. The final precipitate was filtered, washed and dried at room temperature and named as sample M2 after calcination at 550 °C.

Characterizations

The structural analysis of synthesized nanomaterial was done on an AXRD Bench top powder diffraction system with Cu-K α radiation ($\lambda = 0.154\text{nm}$) in between the diffraction angle range 20°-80°. The system was operated at 30.1 KV and 19.1 mA and the scanning angle was varied at an interval of 0.05°.

A UV- Visible spectrophotometer (Unicam - 5625) was used for analyzing the optical properties of synthesized nanoparticles. The experiment was done in a region of wavelength range 325-1100 nm at room temperature. The wavelength was varied in a step of 5nm.

The study of constituent elements and functional groups present in the synthesized sample was done using ABB MB3000 FTIR. The experiment was done in Infra-Red region (400-4000 cm⁻¹) at room temperature.

Sensor fabrication and Response measurements

The sensing response characteristics of manganese oxide nanoparticles were studied using homemade sensor test chamber. The sensor was fabricated on copper electrodes/printed circuit board (PCB) as a substrate. These Cu electrodes were of width 1 mm. The paste of synthesized Mn₂O₃ nanoparticles was uniformly coated onto PCB substrate by screen printing method. Then the thick film was allowed to stabilize at room temperature for 5 h and then annealed at 80 °C for 1 h.

Ammonia gas (NH₃) was introduced into the test chamber using calibrated syringe. The variation in resistance of sensors as a function of gas concentration was recorded by using Keithley current source - nano voltmeter (6221/2182A) at room temperature. The NH₃ gas concentration was varied from 0 ppm -120 ppm. The response time and recovery time were measured in the presence and absence of gas. For the recovery time measurement, the NH₃ gas was removed from the glass chamber by opening the outlet valve. The sensor was heated at 80 °C and cooled to room temperature so that it reached its initial stable resistance value. NH₃ gas of known concentration was injected into the glass chamber and changes in the resistance of sensor were measured at intervals of 1sec through current source -

nano voltmeter (6221/2182A) interfaced with a computer. The sensor response of the sensor for reducing gas is measured by the following formula:

$$\text{Response (\%)} = \frac{\Delta R}{R_a} \quad (1)$$

where, $\Delta R = (R_a - R_g)$, R_a is the resistance of the sensor in the air and R_g is the resistance in the test gas.

Results and discussion

According to the nature of reducing reactants (Sodium hydroxide or hydrochloric acid), the synthesized manganese oxides nanomaterial was named as sample M1 and sample M2. XRD analysis was performed to analyze the crystal structure and crystallite size of the synthesized samples M1 and M2. Both the as grown materials were found to be amorphous and became nanocrystalline after annealing treatment at 550°C for 4 hours.

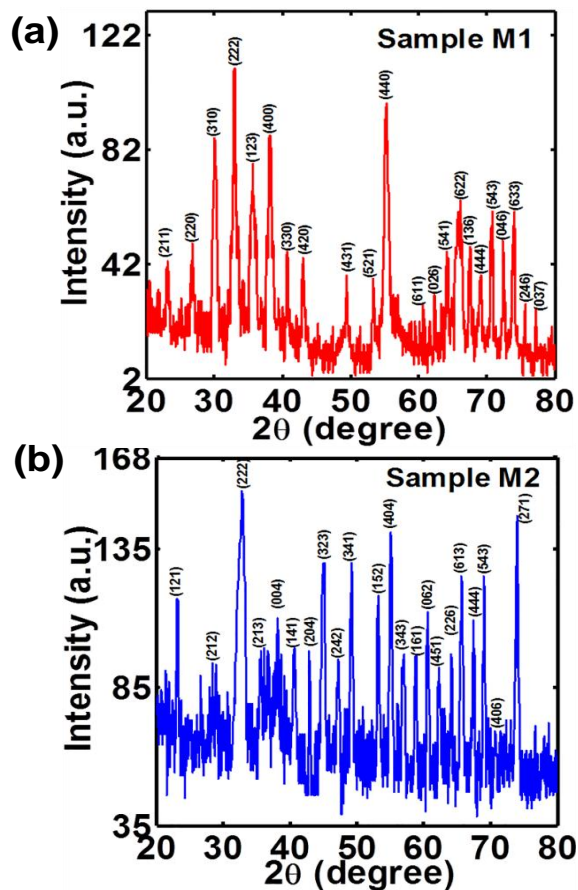


Fig. 1. X-ray diffraction patterns of (a) Cubic Mn_2O_3 nanoparticles, (b) orthorhombic Mn_2O_3 nanoparticles; calcined at 550°C.

Fig. 1(a) shows the XRD pattern of sample M1 (Mn_2O_3 nanoparticles), with broad and well-defined reflections which are in good agreement with the standard peak values of pure Mn_2O_3 (ICDD file no. 76-0150), the corresponding hkl planes are well

indexed to a cubic phase. **Fig. 1(b)** shows the XRD pattern of sample M2 (Mn_2O_3 nanoparticles). Sample M2 shows that all the diffraction peaks measured in the 2θ range correspond to the orthorhombic structure. These peaks are in good agreement to those reported in standard ICDD file no.73-1826. Such a modification in the crystal structure of manganese oxide nanoparticles was observed due to the variation of reducing agent. The crystallite sizes were determined by using the Debye Scherrer's formula which is as follows:

$$D = \frac{0.9\lambda}{\beta \cos \theta} \quad (2)$$

where, D is the crystallite size, λ ($= 0.154 \text{ nm}$) is the wavelength of the incident X-ray radiation, β is the full width at half maxima and θ is the diffraction angle at which the reflection (peak) occurs.

Using the above Scherrer's formula the crystallite size of sample M1 and sample M2 were estimated as 12.56 nm and 11.90 nm respectively. The nanoparticles of these crystallite sizes have high specific surface area. Such a specific characteristic can be beneficial for gas sensing applications.

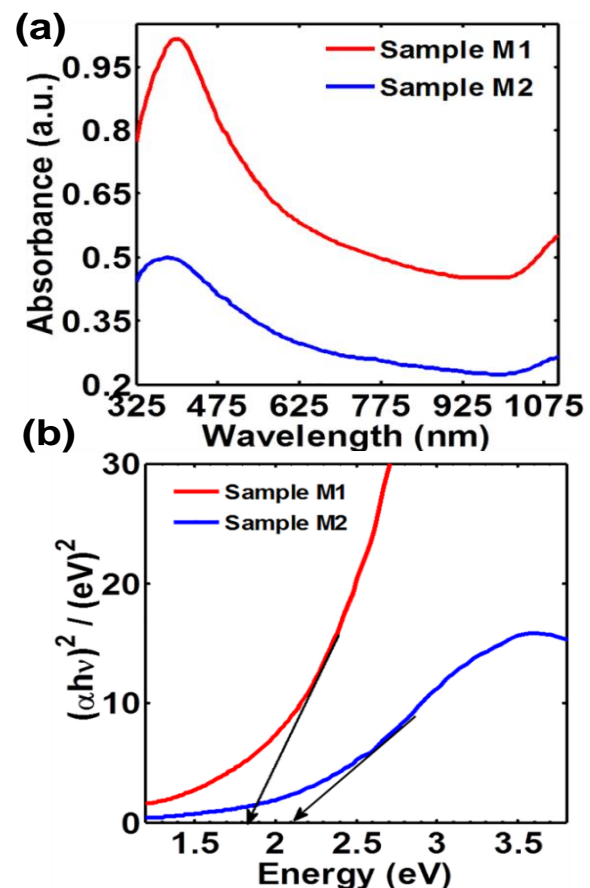


Fig. 2. (a) UV-Visible absorption spectra of sample M1 and sample M2 (b) Tauc plots of $(\alpha h\nu)^2$ versus $h\nu$ of sample M1 and sample M2.

The optical properties of synthesized Mn_2O_3 nanoparticles were studied by UV-Visible spectrophotometer in the range 325-1100 nm. **Fig. 2(a)** shows UV-Visible absorption spectra of sample M1 and sample M2 in UV and visible range. For UV characterization, both samples were dispersed in distilled water at room temperature. From the **Fig. 2(a)**, it can be clearly seen that sample M1 and sample M2 show sharp absorption in the above-defined wavelength range. Such a sharp absorption occurs due to electron excitation from filled to the empty band. The absorption peak was found to be shifted to shorter wavelength for sample M2.

The band gaps of both the samples M1 and M2 were calculated using equation (3). Band gap was measured from the intercept on energy axis obtained by extrapolating the linear portion of the Tauc plot of $(\alpha h\nu)^2$ vs $(h\nu)$ as shown in **Fig. 2(b)**.

$$(\alpha h\nu) = A(h\nu - E_g)^n \quad (3)$$

where, $\alpha = 2.303 A/L$, A is the absorbance of the sample, L is the path length (1 cm), E_g denotes optical band gap energy. The constant 'n' may have value $\frac{1}{2}$ or 2, for the allowed direct or indirect transitions respectively [32].

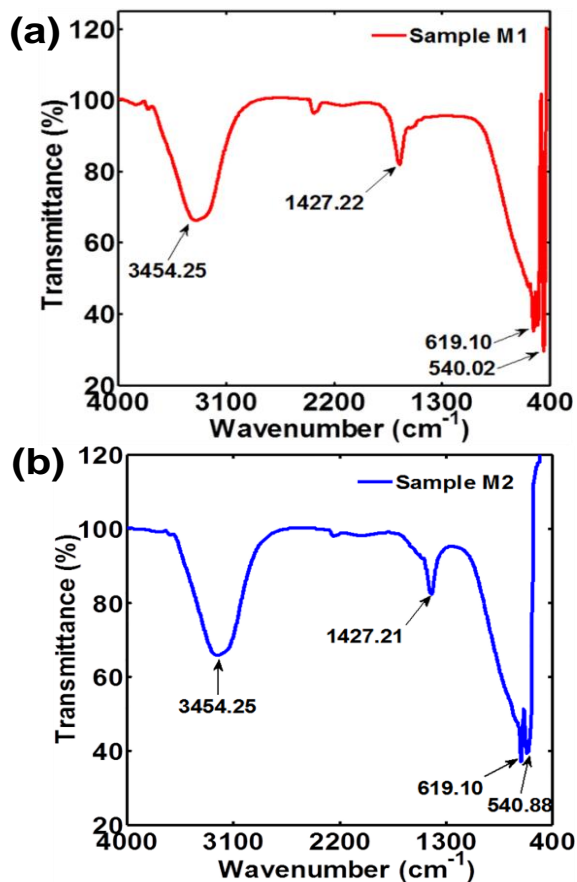


Fig. 3. FT-IR transmission spectra for (a) Cubic Mn_2O_3 nanoparticles (sample M1) (b) orthorhombic Mn_2O_3 nanoparticles (sample M2).

Error in the band gap measurement was $\pm 0.009\text{eV}$. The nature of curve suggested the direct inter band transition. The band gap for sample M1 is found to be 1.8 eV and that of sample M2 is 2.17 eV. These values are close to the reported value of Mn_2O_3 nanoparticles [33]. The band gap of sample M2 is found to be greater than sample M1 which is in confirmation with the smaller crystallite size of sample M2 as determined from XRD. FTIR spectrometry was used to determine the existence of foreign species. The FTIR spectra of samples M1 and M2 are shown in **Fig. 3(a) & 3(b)** respectively. From the figures it can be seen that peaks corresponding to the stretching vibrations of Mn-O and Mn-O-Mn bonds are observed at wavenumbers $540.02\text{ cm}^{-1} - 619.10\text{ cm}^{-1}$ respectively for sample M1. While for sample M2 corresponding wavenumbers are $540.88\text{ cm}^{-1} - 619.10\text{ cm}^{-1}$ [34-35]. Such results confirm the formation of Mn_2O_3 nanoparticles. The peak at the wavenumber 3454.25 cm^{-1} was assigned to O-H stretching vibration of water molecule while the peaks at wavenumbers 1427.21 cm^{-1} and 1427.22 cm^{-1} were assigned to C-C stretching vibrations for sample M1 and sample M2 respectively.

NH_3 sensing performance

To examine scientifically and comparing the NH_3 gas sensing properties of both samples M1 and M2, thick film sensors were designed and tested under different NH_3 gas concentrations in a range 10 - 120 ppm at room temperature.

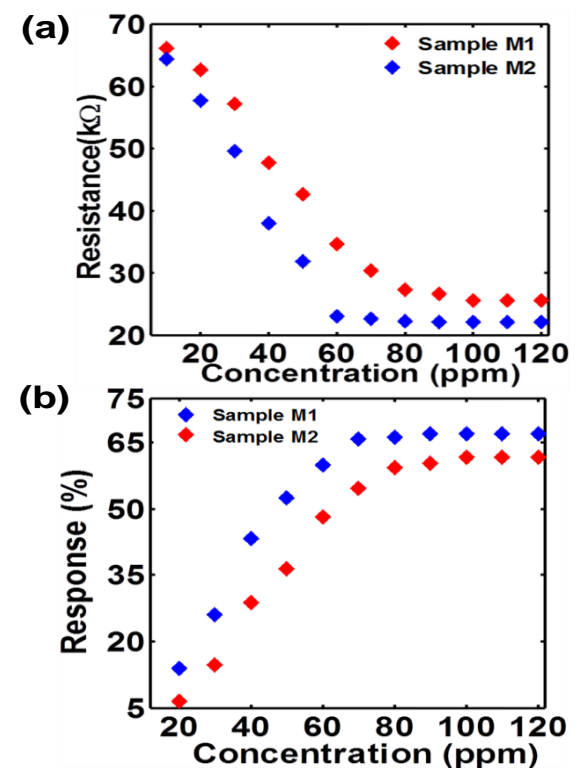
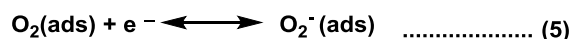


Fig. 4. (a) Variation in resistance with concentration of NH_3 for sample M1 and sample M2 (b) NH_3 response of sample M1 and sample M2 at different concentrations; at room temperature.

Fig. 4(a) shows the variation in resistance with different NH₃ gas concentration for sample M1 and sample M2 based thick film sensors. When the ammonia gas was inserted in the glass chamber, it reacted with the sensor materials. A decrease in resistance of the thick film was observed. Since, it is well known that the performance of sensors is dependent on the strength of the surface interactions between testing gas and the adsorbed oxygen. Initially, when the thick film based sensors were exposed to air, the manganese oxide nanoparticles absorb oxygen molecules on the surface. These adsorbed oxygen molecules get converted into negative oxygen anions by taking an electron from the conduction band of Mn₂O₃ nanoparticles. This process leads to the formation of thick depletion layer at the surface of the Mn₂O₃ thick film and intergranular regions [36-37]. This results in a high resistance value of the Mn₂O₃ films [38-39]. Manganese oxide thick film based sensors are expected to exhibit better properties with large surface to volume ratio and also leads to an improved capacity in absorbing atmospheric oxygen for enhancing the sensor performance [40]. The reactions involved in above defined process are described using the following equations:



We utilized this property to design Mn₂O₃ nanoparticles based thick film sensors for sensing NH₃ gas. When the sensor was exposed to NH₃ gas molecules, they interacted with adsorbed negative oxygen species on the surface of the nanoparticles and in the intergranular regions. During this process trapped electrons come back to the conduction band of the Mn₂O₃ nanoparticles and hence a decrement in resistance of Mn₂O₃ thick film based sensor was observed. During this process, water vapor and gaseous species are produced as an output. The complete reaction mechanism of NH₃ with adsorbed oxygen ion species may occur as shown below:



The response of Manganese Oxide thick film sensors versus NH₃ gas concentration is illustrated in **Fig. 4(b)**. From the figure, it can be clearly seen that the response of both Manganese Oxide thick film based sensors (sample M1 & sample M2) increased gradually with increasing concentration of NH₃ gas up to 80 ppm. When we increased the concentration of NH₃ gas above 80 ppm, negligible variation was recorded. The experiment was repeated many times at room temperature giving same results. On comparing the sensor characteristics, the manganese

oxide thick film based sensor (sample M2) exhibited the good response than that of (sample M1) to NH₃ gas. The maximum sensor response 67.1% was recorded for Manganese oxide thick film based sensors (sample M2) and 61.8% for Manganese oxide thick film based sensors (sample M1). This increment in sensor response may be attributed to the reduction in crystallite size as observed from XRD (**Fig. 1(a) & (b)**) as well as the activation energy. The small crystallite size leads to the large specific area which contributes to the more gas adsorption on the surface of the sensor material and hence responsible for the increase in response. The fulfillment of oxygen ion adsorption and desorption process on the surface of sensor material is also responsible for this enhancement. In our case, Mn₂O₃ nanoparticles are able to sense a low concentration of NH₃ gas at room temperature. The room temperature sensing of NH₃ gas by Mn₂O₃ nanoparticles based sensors can be attributed to the lower activation energy of the reaction between the gaseous molecules and adsorbed Oxide anions on the surface of Mn₂O₃ nanoparticles.

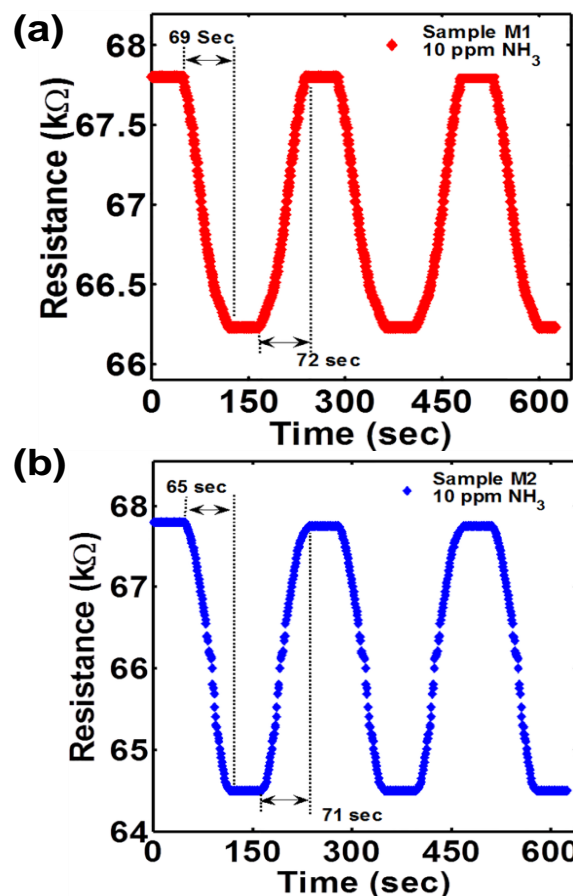


Fig. 5. Variation in resistance with time for (a) sample M1, (b) sample M2; at room temperature.

For recovery time measurement, the unreacted ammonia gas was removed from the glass chamber and the chamber was exposed to air. The response time is measured as the time taken by the thick film

based sensor to acquire the 90% of its minimum resistance value in the presence of NH₃ gas. When the minimum resistance value is attained, NH₃ gas was removed from the glass chamber through its outlet valve and the sensor was allowed to regain its original resistance value. **Fig. 5 (a) & (b)** show the variation in resistance with time for sample M1 and M2 (Manganese Oxide thick film) based sensor operating at room temperature towards 10 ppm NH₃ gas. When the NH₃ gas was introduced into the gas chamber, the sensor resistance drastically decreased up to 66.2 KΩ for sample M1 and 64.5 KΩ for sample M2 slowly and became constant. The response and recovery time of the Manganese Oxide thick film based sensor is found to be 69 sec & 72 sec for sample M1 and 65 sec & 71 sec for sample M2 respectively. The repeatability in the sensor response is checked by testing 10 times the sensor film for 10 ppm concentration of NH₃ gas. A very little variation of ±0.3% was found in the sensor film resistance. The Mn₂O₃ nanoparticle based sensors exhibited good response and low ppm level detection towards NH₃ gas at room temperature.

Conclusion

The structural and optical investigations have confirmed the formation of Mn₂O₃ nanoparticles by chemical co-precipitation method. This method was very simple, cheap and high yielding. The gas sensing characterizations showed that Mn₂O₃ nanoparticles can be used for sensing the NH₃ gas at room temperature. Hence Mn₂O₃ nanoparticles lower the activation energy for reaction between negative Oxide ions and NH₃. Further, the sensing performance of sample M2 was improved as compared to that of sample M1. This improvement in NH₃ gas response could be attributed to a reduction in crystallite size. Our result has a great relevance since the detection of NH₃ gas is very important for disaster management.

Acknowledgements

The authors are thankful to University Grant Commission, New Delhi for the financial support for carrying out this research work and DST for providing FIST grant to Physics department, University of Allahabad.

Author's contributions

Conceived the plan: Pratima Chauhan; Performed the experiments: Shiva Sharma, Shahid Husain; Data analysis: Pratima Chauhan, Shiva Sharma; Wrote the paper: Shiva Sharma, Pratima Chauhan. Authors have no competing financial interests.

References

1. Chauhan, P.; Sharma, S. *J. Nanomed. Res.* **2016**, 3(5), 00067.
2. Pérez-Ramírez, J.; Christensen, C. H.; Egeblad, K.; Christensen, C.H.; Groen, J.C. *Chem. Soc. Rev.* **2008**, 37, 2530.
3. Raghupati, P.; Park, D. H.; Campet, G.; Vasan, H. N.; Hwang, S.J.; Choy, J. H.; Munichandraiah, N. *J. Phys. Chem. C*, **2009**, 113, 6303.

4. Li, Y. S.; Xu, J.; Chao, J. F.; Chen, D.; Ouyang, S.; Ye, J.H.; Shen, G.Z. *J. Mater. Chem.* **2011**, 21, 12852.
5. Han, L.; Wang, D.J.; Cui, J.B.; Chen, L.P.; Jiang, T.F.; Lin, Y.H. *J. Mater. Chem.* **2012**, 22, 12915.
6. Rao, C.N.R., Muller, A.; Cheetham, A.K. (Eds.); Wiley-VCH Verlag GmbH & Co. KGaA. **2005**, pp. 1-11.
7. Ma, X.; Zhu, T.; Xu, L.; G.; Zheng, J.; Liu, A. *Anal. Bioanal. Chem.* **2008**, 390, 1133.
8. Li, F.; Guo, S.; Shen, J.; Shen, L.; Sun, D.; Wang, B.; Chen, Y.; Ruan, S. *Sens. & Act. B.* **2016**, 238, 364.
9. Chauhan, P.; Annapoomi. S.; Tripathi, S. K. *Thin Solid films.* **1999**, 346, 266.
10. Li, P.; Nan, C.; Wei, Z.; Lu, J.; Peng, Q.; Li, Y. *Chem. Mater.* **2010**, 22, 4232.
11. Sharrouf, M.; Awad, R.; Roumie, M.; Marhaba, S. *Mater. Sci. Appl.* **2015**, 6, 850.
12. Zhang, H.; Liang, C.; Tian, Z.; Wang, G.; Cai, W. *J. Phys. Chem. C.* **2010**, 114, 12524.
13. Duay, J.; Stefanie A.; Sherrill, Gui, Z.; Gillette, E.; Lee, S. B. *ACS Nano.* **2013**, 7, 1200.
14. Gnanam, S.; Rajendran, V. *J. Sol-Gel Sci. Technol.* **2011**, 58, 62.
15. Rai, P.; Yu, Y. T. *Sens. & Act. B.* **2012**, 173, 58.
16. Rao, G. S. T.; Rao, D. T. *Sens. & Act. B.* **1999**, 55, 166.
17. Gong, H.; Hu, J.Q.; Wang, J. H.; Ong, C. H.; Zhu, F. R. *Sens. & Act. B.* **2006**, 115, 247.
18. Badadhe, S. S.; Mulla, I. S. *Sens. & Act. B.* **2009**, 143, 164.
19. Delaunay, J. J.; Kakoiyama, N.; Yamada, L. *Mater. Chem. Phys.* **2007**, 104, 141.
20. Liu, Y.; Wang, L.; Wang, H.; Xiong, M.; Yang, T.; Zakharova, G.S. *Sens. & Act. B.* **2016**, 236, 529.
21. Sharma, S.; Chauhan, P. *AIP Conference Proceedings.* **2016**, 1724, 020106.
22. Wang, L.; Lou, Z.; Zhang, R.; Zhou, T.; Deng, J.; Zhang, T. *Appl. Mater. Interfaces.* **2016**, 8 (10), 6539.
23. Balamurugan, C.; Lee, D. W. *Sens. & Act. B.* **2015**, 221, 857.
24. Fang, F.; Bai, L.; Song, D.; Yang, H.; Sun, X.; Sun, H.; Zhu, J. *Sensors.* **2015**, 15, 20086.
25. Ahmad, T.; Ramanujachary, K.V.; Lofland, S.E.; Ganguly, A. K. *J. Mater. Chem.* **2004**, 14, 3406.
26. Gleiter, H. *Acta. Mater.* **2000**, 48, 1.
27. Preisler, E. E. *J. Appl. Electrochem.* **1976**, 6, 311.
28. Lee, G. H.; Huh, S. H.; Jeong, J. W.; Choi, B. J.; Kim, S. K.; Ri, H. C. *J. Am. Chem. Soc.* **2002**, 124, 12094.
29. Kamruddin, M.; Ajikumar, P.K.; Nithya, R.; Mangamma, G.; Tyagi, A. K.; Raj, B. *Powder Technol.* **2006**, 161, 145.
30. Zhang, L.; Zhou, Q.; Liu, Z.; Hou, X.; Li, Y.; Lv, Y. *Chem. Mater.* **2009**, 21, 5066.
31. Gurban, A. M.; Burtan, D.; Rotariu, L.; Bala, C. *Sens. & Act. B.* **2015**, 210, 273.
32. Kang, J.; Tsunekawa, S.; Kasuya, A. *Appl. Surf. Sci.* **2001**, 174, 306-309.
33. Tsunekawa, S.; FuKuda, T.; Kasuya, A. *J. Appl. Phys.* **2000**, 87, 1318.
34. Liu, Y.; Dai, H.; Deng, J.; Zhang, L.; Zhao, Z.; Li, X.; Wang, Y.; Xie, S.; Yang, H.; Guo, G. *Inorg. Chem.* **2013**, 52, 8665.
35. Hongmin, C.; Junhui, H. *J. Phys. Chem. C.* **2008**, 112, 17540.
36. Shukla, T. J. *Sens. Technol.* **2012**, 2, 102.
37. Balamurugan, C.; Lee, D. W. *Sens. Actuators, B.* **2015**, 221, 857.
38. Phani, A.R.; Manorma, S.; Rao, V.J. *Mater. Chem. Phys.* **1999**, 58, 101.
39. Mitra, P.; Chatterjee, A.P.; Maiti H.S. *Mater. Lett.* **1998**, 35, 33.
40. Skapin, S. D.; Kunej, S.; Suvorov, D. J. *Euro. Ceram. Soc.* **2008**, 28, 3119.